THE SEA: THE CURRENT AND FUTURE OCEAN
Journal of Marine Research, 77, Supplement, 215–245, 2019

The ecological and biogeochemical state of the North Pacific Subtropical Gyre is linked to sea surface height

by Benedetto Barone,[1,2,3] Ashley R. Coenen,[4,5] Stephen J. Beckett,[6,7] Dennis J. McGillicuddy, Jr.,[8,9] Joshua S. Weitz,[4,6,10] and David M. Karl[1,11]

ABSTRACT

Sea surface height (SSH) is routinely measured from satellites and used to infer ocean currents, including eddies, that affect the distribution of organisms and substances in the ocean. SSH not only reflects the dynamics of the surface layer, but also is sensitive to the fluctuations of the main pycnocline; thus it is linked to events of nutrient upwelling. Beyond episodic upwelling events, it is not clear if and how SSH is linked to broader changes in the biogeochemical state of marine ecosystems. Our analysis of 23 years of satellite observations and biogeochemical measurements from the North Pacific Subtropical Gyre shows that SSH is associated with numerous biogeochemical changes in distinct layers of the water column. From the sea surface to the depth of the chlorophyll maximum, dissolved phosphorus and nitrogen enigmatically increase with SSH, enhancing the abundance of heterotrophic picoplankton. At the deep chlorophyll maximum, increases in SSH are associated with decreases in vertical gradients of inorganic nutrients, decreases in the abundance of eukaryotic phytoplankton, and increases in the abundance of prokaryotic phytoplankton. In waters below ∼100 m depth, increases in SSH are associated with increases in organic matter and decreases in inorganic nutrients, consistent with predicted consequences of the vertical displacement of isopycnal layers. Our analysis highlights how satellite measurements of SSH can be used to infer the ecological and biogeochemical state of open-ocean ecosystems.

Keywords: biogeochemistry, mesoscale, sea surface height, time series, nutrients, mesoscale eddy

1. Daniel K. Inouye Center for Microbial Oceanography: Research and Education (C-MORE) and Department of Oceanography, 1000 Pope Road, University of Hawaii at Manoa, Honolulu, HI 96822 USA.
2. Corresponding author: ***e-mail: benedetto.barone@gmail.com***
3. Orcid: 0000-0002-1102-7837.
4. School of Physics, Georgia Institute of Technology, 837 State Street, Atlanta, GA 30332 USA.
5. Orcid: 0000-0001-7377-139X.
6. School of Biological Sciences, Georgia Institute of Technology, 310 Ferst Drive, Atlanta, GA 30332 USA.
7. Orcid: 0000-0002-4410-2960.
8. Department of Applied Ocean Physics and Engineering, Woods Hole Oceanographic Institution, 266 Woods Hole Road, Woods Hole, MA 02543 USA.
9. Orcid: 0000-0002-1437-2425.
10. Orcid: 0000-0002-3433-8312.
11. Orcid: 0000-0002-6660-6721.

1. Introduction

It has long been recognized that biological and biogeochemical systems respond to environmental changes that are associated with fluctuations in sea surface height (SSH), ranging in scale from planetary waves (Uz, Yoder, and Osychny 2001) to mesoscale eddies (Robinson et al. 1993). In general, SSH variations reflect the fluctuations of the main pycnocline (Chiswell 1996; Siegel, McGillicuddy, and Fields 1999), a layer that contains high concentrations of inorganic nutrients. For this reason, Siegel, McGillicuddy, and Fields (1999) linked SSH observed at the Bermuda Atlantic Time-series Study site with eddy-induced upwelling of nutrients. Such events were subsequently connected with changes in phytoplankton species composition and export (Sweeney, McGillicuddy, and Buesseler 2003). The studies by Siegel, McGillicuddy, and Fields (1999) and Sweeney, McGillicuddy, and Buesseler (2003) showed how ocean time-series observations offer unique opportunities to quantify the nature of the processes linking SSH and marine ecosystems. However, to our knowledge there has been no systematic study of the relationship between SSH and the suite of biogeochemical measurements taken as part of long-term, ocean time series. Here we present the first such evaluation for the Hawaii Ocean Time-series (HOT), in the North Pacific Subtropical Gyre.

The relative ease of measuring SSH from satellite observations forms the basis for the central question in our study: Is SSH variability linked to changes in the biogeochemical characteristics of marine ecosystems and, if so, how? In order to identify the ecological and biogeochemical changes associated with SSH, we compared 23 years of satellite observations to shipboard observations collected at Station ALOHA (22°45′ N, 158° W), the main sampling site for the HOT program (Karl and Lukas 1996). The HOT observations include vertically resolved, near monthly hydrographic and biogeochemical measurements of seawater properties, thus providing a unique data set to compare with the temporal variability of SSH. We used multiple statistical methods to identify robust changes in marine biogeochemistry linked to variation in SSH.

We do not expect precise correspondence between SSH and upper ocean biogeochemistry because of the multifaceted nature of the potential linkages. In general, variations in SSH reflect vertical displacements of the main thermocline (Wunsch 1997) associated with Rossby waves, eddies, and fronts (Chelton and Schlax 1996; Chelton, Schlax, and Samelson 2011), as well as other phenomena associated with baroclinic instability (Pedlosky 1979). Such disturbances manifest themselves in the structure of the upper ocean, in some cases intensified by interactions with the mean flow (McWilliams 1974). However, the upper ocean is also subject to direct forcing by the atmosphere, resulting in a highly complex environment driven from both above and below. The fact that biological responses to such forcing can be nonlinear further complicates the relationship between SSH and upper ocean biogeochemistry. Nonetheless, we propose that identifying the main biogeochemical changes linked to variation in SSH can be the first step to disentangling these complex physical-biological dynamics.

Modern satellite observations resolve SSH variations associated with mesoscale currents (Morrow and Le Traon 2012), which are the most energetic motions in the ocean (Munk 2002). The energetic dominance of mesoscale motions implies that biogeochemical changes linked to SSH variation represent a considerable fraction of the horizontal variability of open-ocean ecosystems (Doney et al. 2003). For this reason, our study represents an important step toward characterizing the spatial heterogeneity of marine systems and toward understanding the complex dynamics that sustain it.

2. Materials and methods

We used multimission satellite altimetric observations of sea level anomaly (SLA) analyzed and distributed by the Copernicus Marine and Environment Monitoring Service (http://www.marine.copernicus.eu). SLA is the anomaly of SSH with respect to its average computed for the reference period between 1993 and 2012. This SLA was distributed with a daily temporal resolution and a horizontal resolution of 0.25° in latitude and longitude for the period between 1993 and 2015. In order to obtain the time series of SLA at Station ALOHA, we interpolated from the altimetric maps to extract a value for the coordinates of the sampling station. To use the variation of SSH as a proxy for mesoscale variability, we removed the interannual trend caused by sea level change (Church et al. 2013) and the seasonal cycle caused by steric effects (Vinogradov and Ponte 2010) from the time series. The interannual trend was computed with a model I linear regression, and the seasonal cycle was modeled as a sinusoidal whose phase and amplitude were computed using nonlinear least squares regression.

Mesoscale eddies were identified and tracked using the Mesoscale Eddy Trajectory Atlas (version 2.0) distributed by AVISO+ (http://www.aviso.altimetry.fr/). This atlas is based on an algorithm that identifies eddies based on specific criteria applied to space/time variations in SLA (Schlax and Chelton 2016). Among all eddies in the atlas, those traversing Station ALOHA were defined as those having a radius greater than the distance between the eddy centroid and the center of the sampling station (22°45′ N, 158° W). The characteristics of these eddies are described in the Appendix.

Hydrographic and biogeochemical observations from HOT were obtained through the Hawaii Ocean Time-series Data Organization and Graphical System (HOT-DOGS; http://hahana.soest.hawaii.edu/hot/hot-dogs/). The analytical methods used for the different measurements are available online (http://hahana.soest.hawaii.edu/hot/methods/results.html). The biogeochemical measurements compared to SLA were the following: the concentrations of nitrate plus nitrite ($NO_3^- + NO_2^-$), phosphate (PO_4^{3-}), silicate (SiO_4^{4-}), dissolved inorganic carbon (DIC), dissolved oxygen (O_2), fluorometric chlorophyll *a* (chl *a*), particulate carbon and nitrogen (PC and PN), dissolved organic carbon, nitrogen, and phosphorus (DOC, DON, and DOP, respectively); the abundances of heterotrophic picoplankton including bacteria and archaea (het. pico.), *Prochlorococcus* (*Proch.*), *Synechococcus* (*Syn.*), and eukaryotic phytoplankton (euk. phy.); the rates of primary production as estimated through

the assimilation of ^{14}C-labeled bicarbonate (^{14}C-PP); and particle export from the euphotic zone measured using free-drifting sediment traps positioned at a depth of 150 m. For the determination of DOC concentration, we used data starting from 2002 that employed the high-temperature combustion method with a Shimadzu TOC-V CSH instrument. For each HOT cruise, we used the average profile of potential density to compute the depth of 500 isopycnal surfaces from the upper 1,000 m of the water column. These average vertical profiles of potential density are not affected by the tidal and near inertial variability because of the burst conductivity-temperature-depth sampling design of the HOT cruises (Karl and Lukas 1996).

The depths of the base of the mixed layer (ML) and of the deep chlorophyll maximum (DCM) were defined based on vertical profiles of potential density and in situ chlorophyll fluorescence collected on HOT cruises (we took the average value of all the profiles from each cruise). The base of the ML was defined as the first depth below 10 m where the density was at least 0.03 kg m^{-3} greater than the density at 10 m (de Boyer Montégut et al. 2004). We defined the depth of the DCM as the maximum fluorescence on profiles passed through a running median filter with a vertical window of 5 m to remove small-scale vertical variability.

The comparison between biogeochemical measurements and SLA was made at eight depth levels following the HOT sampling scheme. Each depth bin contained data in a 6 m depth interval centered at 5, 25, 45, 75, 100, 125, 150, and 175 m. DON and DOP measurements followed a different sampling scheme, so we used a bin width of 14 m at the 100 m depth level for these measurements to increase the number of observations. The average number of data points per depth bin for each biogeochemical variable is reported in Table A3 (Appendix).

A model II geometric mean model was used to compute the slopes of the linear regression between isopycnal depth and SLA. Water density changes seasonally in layers close to the surface so that the least dense isopycnal surfaces were not always observed at Station ALOHA. We only analyzed the results of those regressions for which less than 5% of the observations were missing (1,024.12–1,027.34 kg m^{-3}) in order to avoid a seasonal bias. Spearman's rank correlation coefficient was used to assess the strength of monotonic relationships between HOT biogeochemical observations and SLA, and we used the Benjamini and Hochberg (1995) approach for multiple significance testing (using a false discovery rate of 0.05 and P values from Table A4 in the Appendix). Median values were compared using a Wilcoxon rank sum test and the same approach as given previously for multiple testing.

3. Results

The rate of sea level rise at Station ALOHA for the period 1993–2015 was found to be 1.5 ± 0.1 mm y^{-1} (Fig. 1a). This value is lower than the rate reported for the North Pacific basin of 2.4 ± 0.1 mm y^{-1} from 1993 to 2013 (Fang and Zhang 2015) but is consistent

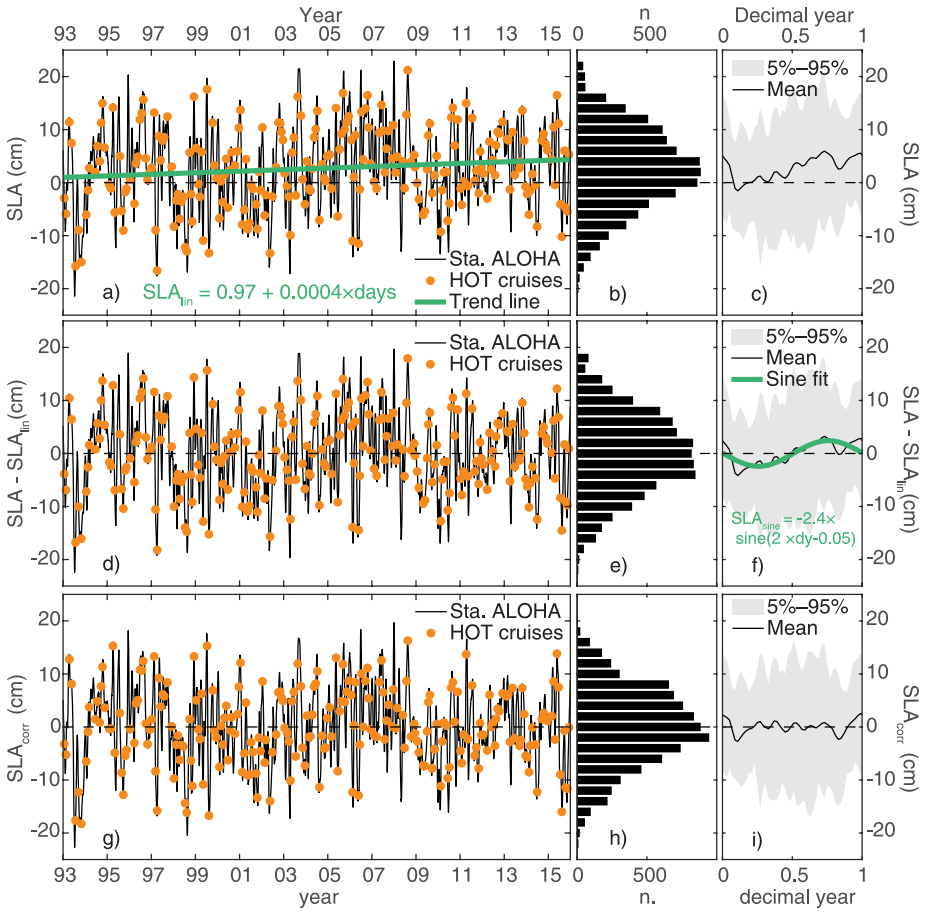

Figure 1. Analysis of sea level anomaly (SLA) at Station ALOHA between 1993 and 2015. Top panels show the original SLA time series (a), its empirical distribution (b), and its seasonal cycle (c). Central panels are as top panels but for the SLA signal after removing the interannual linear trend. Bottom panels are as top panels but for the SLA signal after removing the interannual linear trend and the sinusoidal seasonal cycle. Solid black lines in panels (a), (d), and (g) are daily SLA value, and circles depict SLA at the time of the Hawaii Ocean Time-series (HOT) cruises. Panels (b), (e), and (h) are histograms reporting the frequency of observation of daily SLA values between 1993 and 2015. Panels (c), (f), and (i) depict the seasonal cycle of SLA: solid black lines depict mean SLA values, and gray contours include 90% of the data. Decimal year represents the time from the beginning of the year (1 January at 00:00) divided by the total length of the year. Green lines in panels (a) and (f) depict model fits for the linear trend and the sinusoidal cycle, respectively. The intercept of the regression in panel (a) depicts the value at the beginning of the time series (1 January 1993), and the slope is for time expressed in days. The sinusoidal fit in panel (f) is for time expressed in decimal year (dy).

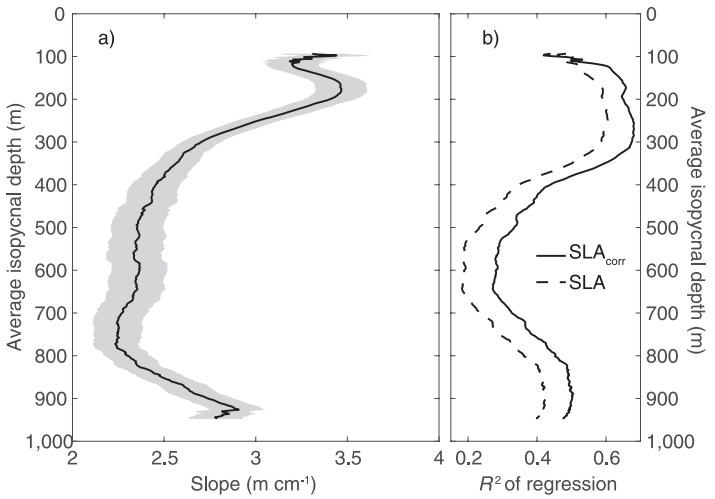

Figure 2. Results from the model II linear regression of isopycnal depth versus sea level anomaly (SLA): (a) slopes of the regression for isopycnal layers from different average depths versus SLA_{corr} and (b) coefficients of determination for the regressions versus SLA (dashed line) and SLA_{corr} (solid line). The gray region in panel (a) depicts the slope plus or minus its standard deviation.

with the rate estimated for the city of Honolulu for the approximate period 1900–1990 using tide gauges (Wyrtki 1990). After removing the linear trend from the signal (Fig. 1d), we computed a sinusoidal seasonal cycle of SLA with a summer maximum and a 2.4 cm amplitude (Fig. 1f), consistent with an earlier estimate reporting an amplitude <3 cm near Station ALOHA (Mitchum 1996). We then defined SLA_{corr} as the SLA signal corrected for both the linear trend and the seasonal cycle. The characteristics of this new variable are shown in Figure 1(g)–(i).

The depth of isopycnal surfaces increased with SLA, as shown by positive slopes of the linear regressions (Fig. 2a), and the power of these regressions increased when using SLA_{corr} rather than uncorrected SLA (Fig. 2b). Slopes were in the 2.2–3.5 m cm^{-1} range and 27%–68% of the variance of isopycnal depth was explained by variations of SLA_{corr} (Fig. 2). The greatest slopes were measured in the layer between ~100 and ~250 m (Fig. 2a).

The biogeochemical observations from the upper 175 m of the water column showed many significant positive and negative correlations with SLA_{corr} (Table 1), indicating an increase or decrease, respectively, of the biogeochemical parameter with SSH.

The highest correlation coefficients were found in the 125–175 m layer where the concentration of inorganic nutrients ($NO_3^- + NO_2^-$, PO_4^{3-}, SiO_4^{4-}, and DIC) decreased with SLA_{corr}, whereas particulate organic matter, dissolved organic matter, chl *a*, and heterotrophic picoplankton generally increased with SLA_{corr}.

Table 1. Spearman correlation coefficients of biogeochemical parameters versus SLA_{corr}. An empty cell indicates that the relationship is not significant according to the Benjamini and Hochberg (1995) procedure. ^{14}C-PP, primary production estimated through assimilation of ^{14}C-labeled bicarbonate; Chl *a*, fluorometric chlorophyll *a*; DIC, dissolved inorganic carbon; DOC, DON, and DOP, respectively dissolved organic carbon, nitrogen, and phosphorus; Euk. Phy., eukaryotic phytoplankton; Het. Pico., heterotrophic picoplankton; $NO_3^- + NO_2^-$, nitrate plus nitrite; O_2, dissolved oxygen; PC and PN, particulate carbon and nitrogen, respectively; PO_4^{3-}, phosphate; *Proch.*, *Prochlorococcus*; SiO_4^{4-}, silicate; SLA, sea level anomaly; *Syn.*, *Synechococcus*.

	Depth levels							
Biogeochemical parameters	5 m	25 m	45 m	75 m	100 m	125 m	150 m	175 m
$NO_3^- + NO_2^-$					−0.33	−0.34	−0.56	−0.55
PO_4^{3-}	0.21	0.41	0.33	0.28	0.3		−0.41	−0.5
SiO_4^{4-}				−0.23	−0.27	−0.36	−0.54	−0.59
DIC	−0.21	−0.26	−0.34	−0.39	−0.43	−0.55	−0.38	−0.51
O_2			−0.27				0.17	
Chl *a*						0.12	0.15	0.15
PC				0.16	0.16	0.19	0.16	0.2
PN		0.15		0.19	0.22	0.32	0.27	0.32
DOC			0.28	0.36	0.36	0.4	0.34	0.39
DON				0.26	0.21	0.38	0.35	
DOP					0.26	0.27	0.26	0.3
Het. Pico.		0.18	0.19	0.24	0.21	0.28	0.38	0.31
Proch.					0.24	0.17		
Syn.					0.18			
Euk. Phy.					−0.2			
^{14}C-PP								

In the layer between the sea surface and 100 m depth, the most pronounced patterns were an increase in PO_4^{3-} and a decrease in DIC with SLA_{corr}. Heterotrophic picoplankton abundance increased with SLA_{corr} at all depths but 5 m; some particulate and dissolved organic matter stocks also increased with SLA_{corr}, but more markedly between 75 and 100 m. Conversely, the concentration of chl *a* did not show significant correlations with SLA_{corr} in the upper 100 m. The only significant correlations of O_2 with SLA_{corr} were at 45 m (negative) and at 150 m (positive).

The community around the DCM (114 m on average) changed with SLA_{corr}: *Prochlorococcus* abundance increased with SLA_{corr} at 100 and 125 m, *Synechococcus* abundance increased with SLA_{corr} at 100 m, and eukaryotic phytoplankton abundance decreased with SLA_{corr} at 100 m depth. The depths of the DCM and of the base of the ML increased with SLA_{corr}, with correlation coefficients of 0.24 ($P = 0.0003$) and 0.18 ($P = 0.006$), respectively. Rates of primary production in the upper 175 m of the water column did not

correlate with changes of SLA_{corr} nor did fluxes of particles collected by sediment traps at 150 m depth in terms of carbon, nitrogen, and phosphorus.

To evaluate the generality of the correlations that we identified in Table 1, we investigated whether these correlations are robust when accounting for seasonal variations, autocorrelation, and the presence of mesoscale eddies. To test for the effect of the seasonal signal, we calculated the correlations as in Table 1, but after subtracting the monthly mean from each point of the time series. This analysis did not consistently improve the correlations in Table 1, so we do not report those results. To test for the effect of autocorrelation, we accounted for nonindependence between time-series measurements by computing the correlation coefficients on the residuals of an autoregressive model. This analysis (described in the Appendix) complements the results of the direct correlations (Table A5 in the Appendix), providing additional support for the validity of the identified correlations.

We then investigated if the biogeochemical changes of Table 1 were only detected when Station ALOHA was traversed by mesoscale eddies as defined by the eddy tracking criteria. Qualitative analysis of SLA maps indicated considerable mesoscale variability unexplained by identified eddies. To adopt a quantitative approach, we partitioned the time series into two subsets of observations made of (1) days when Station ALOHA was traversed by a mesoscale eddy and (2) days when no eddy was detected. We found that eddies were detected during 31% of the days, but they accounted for 47% of the variance of SLA_{corr} of the entire time series. Eddies contributed disproportionately to this variance because the distribution of SLA_{corr} inside tracked eddies contained higher amplitude fluctuations than periods when no eddies were detected (Fig. 3a). Furthermore, values near the tails of the distribution were more frequently observed inside eddies than values near the mode of the distribution (Fig. 3b). We then used the two subsets of observations, inside and outside tracked eddies, to perform separate correlation analyses between SLA_{corr} and biogeochemical parameters. The correlations found for both subsets of data (Tables A1 and A2 in the Appendix) are similar to those reported for the entire data set (Table 1). These results confirm that the correlations of Table 1 are robust and are not only observed inside identified eddies, but also apply to a wide range of SLA variability (Fig. 3b).

In order to visualize differences in concentration and abundance between periods of high and low SLA, we defined two subsets of measurements: high SLA for $SLA_{corr} > 5$ cm and low SLA for $SLA_{corr} < -5$ cm, corresponding approximately to the highest and lowest quartile of the HOT SLA_{corr} distribution (22% and 26% of the 1993–2015 HOT cruises, respectively). We then calculated the median and the 25th and 75th percentile for high and low SLA data sets for each of the biogeochemical measurements considered in Table 1. This analysis, shown in Figure 4, supports many of the patterns described in the correlation analysis against SLA_{corr}. For example, periods of high SLA had lower concentrations of inorganic nutrients below 100 m (Fig. 4a–c), higher phosphorus concentrations in the upper 100 m (Fig. 4b), and more prokaryotic phytoplankton at 100 m depth (Fig. 4m and n).

To further probe potential biogeochemical drivers suggested via the correlation analysis, we focused on the surface stocks of dissolved nitrogen and phosphorus in the upper 100 m

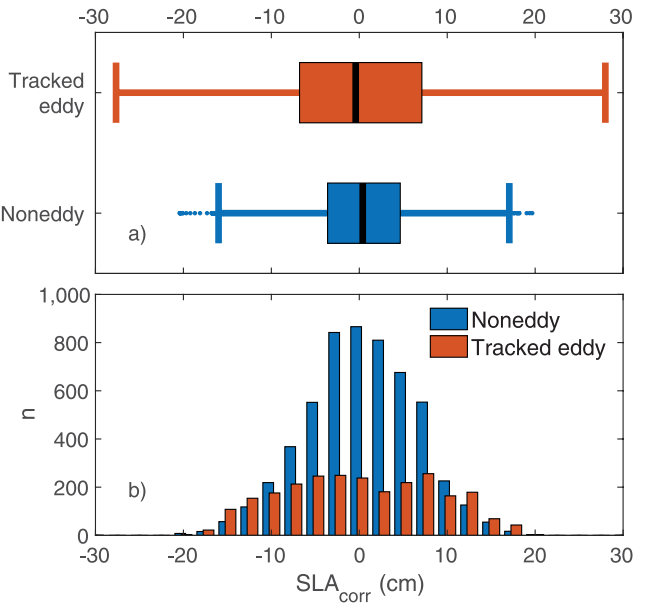

Figure 3. Distribution of SLA_{corr} at Station ALOHA between 1994 and 2015. (a) Box plots of the distribution of SLA_{corr} during days when a tracked eddy traversed Station ALOHA (top) and during days when no eddy traversed Station ALOHA (bottom). Boxes include observations between the first and third quartiles; whiskers include observations between the first quartile minus 1.5 times the interquartile range and the third quartile plus 1.5 times the interquartile range; symbols are observations not included between the whiskers; black vertical lines are median values of the distributions. (b) Histograms of the frequency of SLA_{corr} observations during days when a tracked eddy traversed Station ALOHA (red bars) and during days when no eddy traversed Station ALOHA (blue bars). SLA, sea level anomaly.

of the water column. Despite the different median profiles of DON and DOP between conditions of high and low SLA (Fig. 4j and k), differences were only significant for a few of the eight depth levels taken into account, both in the correlation analysis (Table 1) and in the comparison of the extreme quartiles (Fig. 4j and k). The unclear pattern of variability of DON and DOP in the upper 100 m is presumably because of the short time series (Table A3 in the Appendix) and the relatively low precision associated with these measurements. To circumvent this problem, we calculated the 0–100 m integral concentration of DON and DOP for the entire time series. We then calculated the correlation of the integral concentrations with SLA_{corr}, and we tested the difference between the median integral values for $SLA_{corr} > 5$ cm and $SLA_{corr} < -5$ cm (Table 2). We did the same calculations for inorganic nitrogen and phosphorus ($NO_3^- + NO_2^-$ and PO_4^{3-}), and for total dissolved nitrogen (TDN) and total dissolved phosphorus (TDP), which include both organic and inorganic forms (Table 2). We found that the 0–100 m integral concentrations of PO_4^{3-}, DON, TDN, and TDP significantly

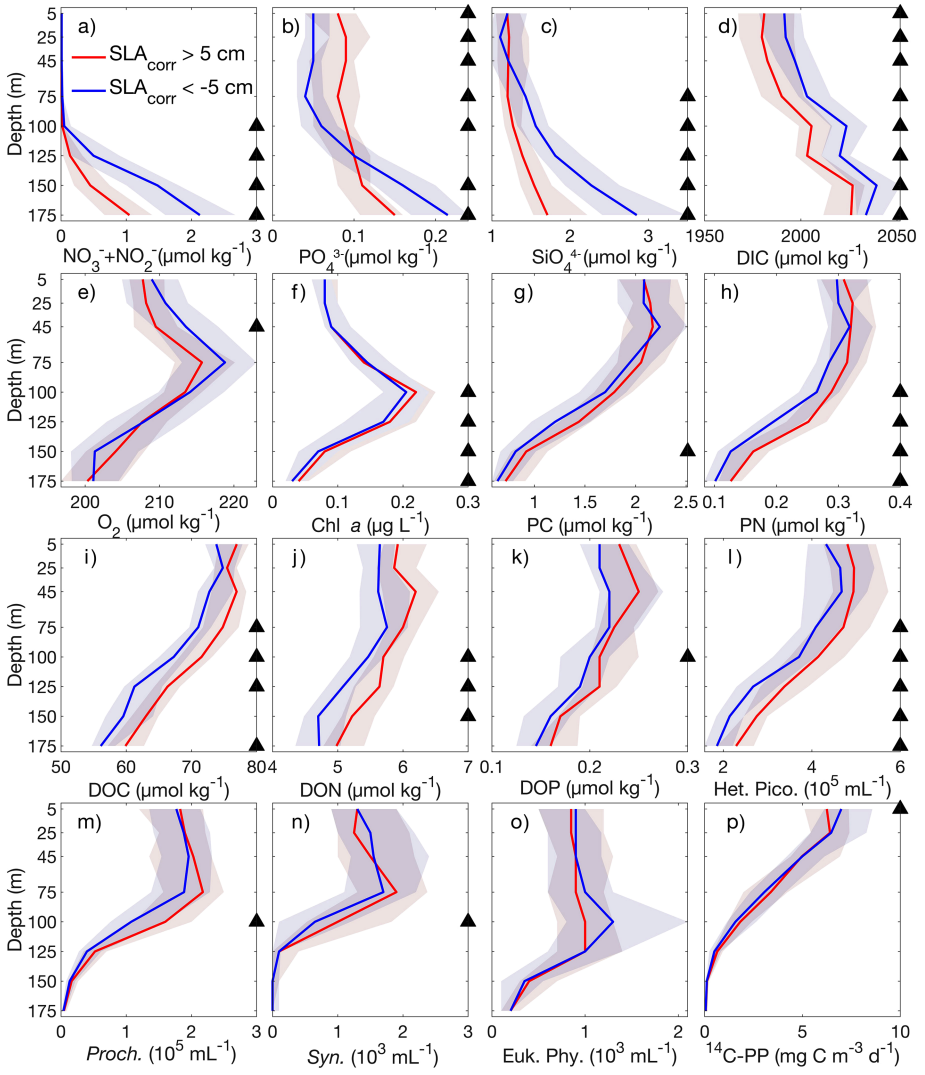

Figure 4. Median vertical profiles of the biogeochemical parameters reported in Table 1 and after selecting data from cruises with $SLA_{corr} > 5$ cm (red line) or $SLA_{corr} < -5$ cm (blue line). The area around the median line encloses data between the 25th and the 75th percentile. Black triangles on the right side of each panel indicate those depths where median values are significantly different according to the Benjamini and Hochberg (1995) procedure. ^{14}C-PP, primary production estimated through assimilation of ^{14}C-labeled bicarbonate; Chl *a*, fluorometric chlorophyll *a*; DIC, dissolved inorganic carbon; DOC, DON, and DOP, respectively dissolved organic carbon, nitrogen, and phosphorus; Euk. Phy., eukaryotic phytoplankton; Het. Pico., heterotrophic picoplankton; $NO_3^- + NO_2^-$, nitrate plus nitrite; O_2, dissolved oxygen; PC and PN, particulate carbon and nitrogen, respectively; PO_4^{3-}, phosphate; *Proch., Prochlorococcus*; SiO_4^{4-}, silicate; SLA, sea level anomaly; *Syn., Synechococcus*.

Table 2. Changes in the 0–100 m integral concentration of dissolved N and P with SLA_{corr}. The second column is the Spearman correlation coefficient whose value is not reported if the correlation is not significant. The third and fourth columns report the integral concentration (average ± standard deviation in mmol m^{-2}) of the dissolved stocks in conditions of low and high sea surface height. Bold values represent significant differences between median values at high and low SLA_{corr}. Significance is assessed through the Benjamini and Hochberg (1995) procedure. DON and DOP, dissolved organic nitrogen and phosphorus, respectively; $NO_3^- + NO_2^-$, nitrate plus nitrite; PO_4^{3-}, phosphate; SLA, sea level anomaly; TDN and TDP, total dissolved nitrogen and phosphorus, respectively.

	Correlation coefficient	Concentration $SLA_{corr} > 5$ cm	Concentration $SLA_{corr} < -5$ cm
$NO_3^- + NO_2^-$	−0.2	1.6 ± 1.6	3.9 ± 6.0
PO_4^{3-}	0.33	**8.7 ± 3.5**	**5.6 ± 2.4**
DON	0.26	**616 ± 36**	**584 ± 42**
DOP		24.3 ± 2.5	22.9 ± 3.6
TDN	0.26	**618 ± 36**	**586 ± 41**
TDP	0.29	**32.3 ± 4.2**	**29.0 ± 3.6**

increased with SLA_{corr} and were significantly different between conditions with $SLA_{corr} > 5$ cm and $SLA_{corr} < -5$ cm (Table 2).

4. Discussion

The vertical displacement of water layers associated with mesoscale dynamics provides an important fraction of the new nitrogen to the community of the euphotic layer and is linked to transient and episodic increases in new and export production (Falkowski et al. 1991; McGillicuddy et al. 1998; Uz, Yoder, and Osychny 2001; Benitez-Nelson et al. 2007). Although there is evidence of these episodic events in the North Pacific Subtropical Gyre (Ascani et al. 2013), it is unclear if mesoscale dynamics are also associated with longer-term changes in the ecological and biogeochemical characteristics of the ecosystem. Here, we looked for these changes by comparing SSH from satellite radar observations to hydrographic and biogeochemical observations from HOT, an important open-ocean time series. From the hydrographic comparison, we found that the depth of isopycnal surfaces changed with corrected sea level anomaly, SLA_{corr}, by 2.2–3.5 m cm^{-1} (Fig. 2a). As a comparison, Church et al. (2009) had previously calculated changes of 2.3 m cm^{-1} for the 1,024.6 kg m^{-3} isopycnal (vs. our 3.3 ± 0.1 m cm^{-1} for the same isopycnal), while Siegel, McGillicuddy, and Fields (1999) reported a typical change of 4 m cm^{-1} for the Sargasso Sea.

In the comparison of SLA_{corr} with biogeochemical measurements, we observed patterns driven by the vertical displacement of water layers associated with changes of SLA_{corr}. For example, the concentrations of inorganic nutrients including $NO_3^- + NO_2^-$, PO_4^{3-}, SiO_4^{4-}, and DIC typically increase with depth, so they also decrease with SLA_{corr} in deep waters. The shallowest depth where this change was observed depends on the inorganic nutrient

type (with a minimum of 5 m for DIC and a maximum of 150 m for PO_4^{3-}) because vertical gradients are different for different nutrients, but they are generally weaker close to the surface where no change with SLA_{corr} is detected. Conversely, particulate organic matter, dissolved organic matter, chl *a*, and heterotrophic picoplankton generally increased in deep waters with SLA_{corr}, because of their vertical distribution with higher concentrations at shallower depths.

However, we also identified biogeochemical changes correlated with SLA_{corr} that cannot be interpreted in terms of the vertical displacement of layers of water. One of these changes is the increase of TDN and TDP with SLA_{corr} in the upper 100 m of the water column (Table 2). Changes in phosphorus concentration were mostly because of PO_4^{3-}, whereas changes in nitrogen were because of changes in DON (Table 2). The integral concentrations of TDN and TDP changed by ∼5% and ∼10%, respectively, between conditions of low and high SSH (Table 2). The higher surface concentrations of TDN and TDP in conditions of high SSH are surprising because in this environment the deep stocks of both elements are found farther from the sea surface (TDN = Fig. 4a + Fig. 4k; TDP = Fig. 4b + Fig. 4l).

One mechanism that could potentially explain this phenomenon is the transport of surface water from different regions of the ocean by nonlinear mesoscale eddies, which can trap and transport water for long distances (Zhang, Wang, and Qiu 2014). Eddies with opposite sense of rotation are associated with maxima and minima of SLA, and they have been shown to have different propagation characteristics on a global statistical basis (Chelton, Schlax, and Samelson 2011). Consequently, different eddies could entrap water with different nitrogen and phosphorus concentrations at the moment of their generation, thus potentially explaining the change in concentration with SLA. We tested this hypothesis by examining the trajectories of all eddies that traversed Station ALOHA during the study period (Fig. 5a). We found that eddies traversing Station ALOHA generally originated east of it and were last detected west of it, but the coordinates of origin and last detection were variable. Eddies were also tracked back in time for up to 150 days from the date of their first detection at Station ALOHA. When tracking back eddies of opposite polarity, we observed that they propagated from similar regions of the ocean and at similar speeds (Fig. 5b). Furthermore, the average coordinates of eddy origin were similar between eddies of opposite polarity (Fig. A2 in the Appendix). Thus, we find no evidence to support the hypothesis that water transport by mesoscale eddies causes changes in the surface concentration of N and P with SSH.

These results are consistent with the conclusions of an earlier analysis (Nolan 2008) that found similar translation speed and direction for both cyclones and anticyclones passing through Station ALOHA. At present, the cause of the covariability of N and P concentrations with SLA (Fig. 4) remains enigmatic, but given the important role of these elements in limiting phytoplankton growth, we suggest that future investigations should aim to understand the mechanisms linking the observed changes to SSH and mesoscale dynamics.

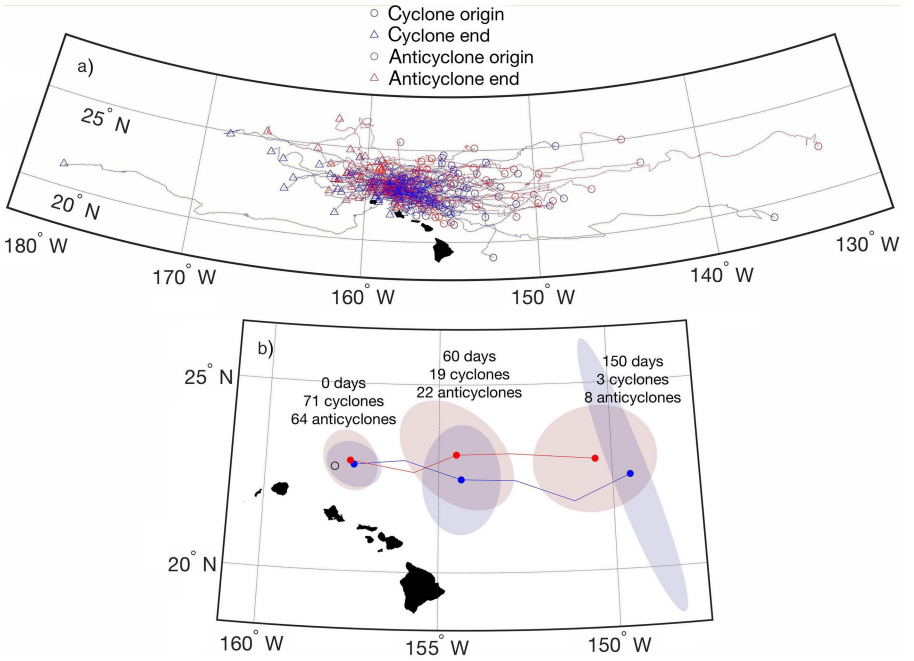

Figure 5. Displacement of the eddies that traversed Station ALOHA. (a) Trajectories of the eddies that traversed the center of Station ALOHA for at least 1 day; circles and triangles depict eddy origin and last detection, respectively. Cyclones are blue, and anticyclones are red. (b) Coordinates of mesoscale eddies at different times before the day when they first traversed Station ALOHA. Blue depicts the position of cyclones, and red the position of anticyclones. Circles are centered at the time of first detection at ALOHA and at 60 and 150 days before then. Shaded ellipses depict the variability of eddy position associated with one standard deviation.

In terms of phytoplankton abundance, we observed an increase in eukaryotic phytoplankton during low SLA_{corr} conditions at 100 m depth (Fig. 4o, Table 1), coincident with the depth of the DCM layer in average profiles (Fig. 4f). We propose that this change in phytoplankton community composition with SSH is linked to the supply of inorganic nitrogen from below (Fig. 4a). To test this hypothesis, we estimated diapycnal and along-isopycnal diffusive rates of $NO_3^- + NO_2^-$ at 100 m depth for conditions of low and high SSH, and we also compared the total flux of inorganic nitrogen in the euphotic zone because of diapycnal fluxes and isopycnal uplifting. A more detailed discussion of the methodology can be found in the Appendix. We found that (1) along-isopycnal fluxes contribute less than diapycnal fluxes to the rate of nutrient diffusion at 100 m; (2) diapycnal fluxes at the DCM are likely to increase at low SSH because of the increased vertical gradient in nutrient concentration; and (3) diapycnal mixing contributes only a small fraction of the inorganic nitrogen flux to the euphotic zone linked to changes in SSH, which is mostly caused by isopycnal uplift (see

the Appendix). These findings support our hypothesis that changes in the phytoplankton community at the DCM are associated with changes in the supply of inorganic nutrients.

Although diapycnal mixing contributes a small fraction of the total nutrient flux associated with mesoscale features, it may play an important role in sustaining enhanced populations of eukaryotic phytoplankton at the DCM, after the isopycnal uplift associated with initial formation and/or intensification of the mesoscale feature. This mechanism is consistent with previous measurements of the isotopic composition of plankton that indicate that eukaryotic phytoplankton dominate nitrate assimilation in the Sargasso Sea (Fawcett et al. 2011). Consistently, in our study, not all phytoplankton taxa respond in the same way to changes in nutrient supply. For example, *Prochlorococcus* and *Synechococcus* variability is the opposite of that observed for eukaryotic phytoplankton: their cells increase in abundance near the DCM in high SSH conditions (Fig. 4m and n, Table 1), which are associated with low $NO_3^- + NO_2^-$ (Fig. 4a) and high DON (Fig. 4j). Opposite variation of prokaryotic and eukaryotic phytoplankton with SSH at 100 m may be a result of eukaryotic phytoplankton outcompeting prokaryotic phytoplankton in conditions of high diapycnal nutrient flux at the DCM.

Despite the vertical displacement of growth-limiting nutrients in the water column, the rate of primary production and particle export did not change with SSH. This observation is not entirely surprising because primary production and particle export should not change in relation to the position of the pycnocline, which changes with SSH, but in relation to the rate of nutrient supply to the euphotic zone. Indeed, the largest delivery of nutrients to the euphotic zone does not take place when isopycnals are at their shallowest depth, but when isopycnals are uplifted during SSH decrease (Appendix). Consequently, it is when SSH decreases that we expect primary production to increase. What is surprising is that primary production did not change with SSH at the depth of the chlorophyll maximum, where the diapycnal flux of nutrients decreases with SSH (Appendix). We hypothesize that increasing diapycnal fluxes are compensated by increasing rates of net community production that are not associated with increasing rates of gross primary production (which is closer to the quantity measured with ^{14}C-PP). In other terms, we propose that the net synthesis of organic matter increases while the overall photosynthetic rate is constant. Because the rate of particle gravitational settling did not change with SSH, we also propose that the new material produced at the DCM could be partly exported by diel vertical migrators (Hannides, Drazen, and Popp 2015), whose abundance has been previously observed to change within mesoscale eddies (Landry et al. 2008; Eden et al. 2009).

In our analysis, we worked under the assumption that different kinds of mesoscale motions have the same qualitative characteristics, whereby higher SSH is linked to deeper isopycnal surfaces. However, there are mesoscale features with different characteristics: mode water eddies deflect the main thermocline downward (causing anticyclonic rotation and positive SLA), but they have shallower isopycnal surfaces near the depth of the seasonal pycnocline (McGillicuddy et al. 2007). Consequently, the biogeochemical characteristics of mode water eddies could be different from normal anticyclones. Mode water eddies

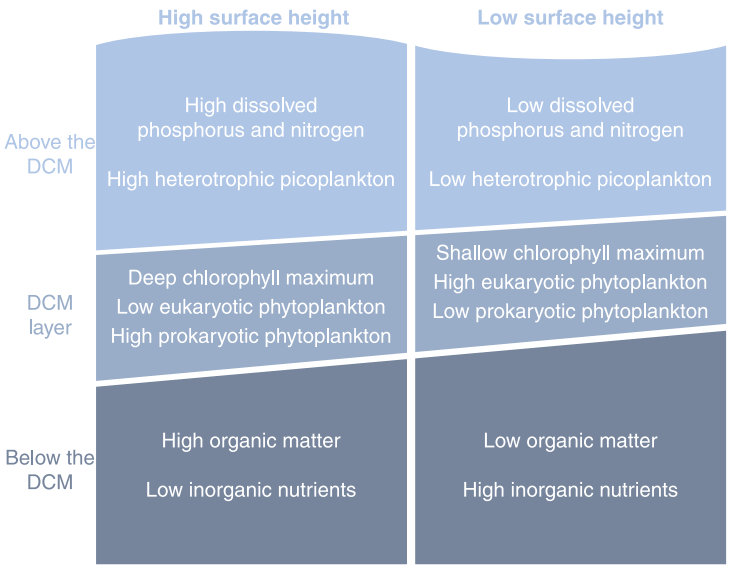

Figure 6. Conceptual representation of the biogeochemical differences between high (left side) and low (right side) sea surface height conditions in three depth layers. DCM, deep chlorophyll maximum.

traversed Station ALOHA during several HOT cruises, and they accounted for ∼16% of all anticyclones (F. Santiago-Mandujano, J. Smith, R. B. Lukas, and D. McCoy, unpublished). When excluding the observations from HOT cruises associated with mode water eddies (13 cruises identified by Santiago-Mandujano et al. between 1993 and 2012) from our analysis, we still observe correlations with similar strength for the main biogeochemical changes identified in Table 1 of this study (data not shown). Specifically, we still observe similar correlations for the increase in phosphorus with SSH in the upper 100 m, for the decrease in inorganic nutrients with SSH below ∼75 m, and for changes in the community composition with SSH at 100 m. These results may imply that mode water eddies were too infrequent to impact the reported correlations or that SSH variation associated with mode water eddies is linked to the same biogeochemical changes observed for the entire time series.

In summary, we identified three depth layers that responded differently, but predictably, to variations of SSH at Station ALOHA (Fig. 6). The first layer extends from the sea surface to ∼100 m depth, or just above the depth of the DCM, where dissolved stocks of nitrogen and phosphorus increase with SSH, and so does the abundance of heterotrophic picoplankton. The second layer is associated with the DCM, whose depth increases with SSH. In the DCM layer, the vertical gradient of inorganic nitrogen concentration decreases with SSH, and this change is linked with a decreased abundance of eukaryotic phytoplankton and an increased abundance of prokaryotic phytoplankton. Below the DCM, we identified a third

layer where inorganic nutrients decrease while organic matter increases with SSH because of the vertical displacement of isopycnal layers.

5. Conclusions

Leveraging multiple decades of measurements, we find that variations in SSH are linked to changes in the concentrations of growth-limiting nutrients and in the abundance of key plankton groups. We propose explanations for some of these variations—for example, that the rate of diapycnal nutrient supply decreases with SSH and this leads to a change in the phytoplankton community composition at the DCM. However, the mechanistic drivers of the variation of other parameters with SSH are still unclear. For example, the change in the surface stocks of dissolved nitrogen and phosphorus with SSH remains unexplained. Future investigations should design sampling and experiments to understand the causes and ecological consequences of the link between SSH, mesoscale dynamics, community composition, and ocean biogeochemistry. In the near term, the observations from this study allow us to translate the daily satellite estimates of SSH variation into baseline predictions of biogeochemical and ecological characteristics of the North Pacific Subtropical Gyre.

Acknowledgments. We thank Andrei Natarov (University of Hawaii) for helpful discussion regarding isopycnal diffusion. This research was supported by the Simons Foundation (SCOPE award #329108 to DMK and JSW), the Gordon and Betty Moore Foundation (grant #3794 to DMK), the National Science Foundation through grants to the Center for Microbial Oceanography: Research and Education (EF-0424599 to DMK) and HOT (OCE-1260164 to DMK), and the 2015 Balzan Prize to DMK. DJM gratefully acknowledges support from the National Science Foundation and the National Aeronautics and Space Administration.

SLA is distributed by the Copernicus Marine and Environment Monitoring Service (http://www.marine.copernicus.eu). HOT observations are available through HOT-DOGS (http://hahana.soest.hawaii.edu/hot/hot-dogs/). The Mesoscale Eddy Trajectory Atlas is produced by SSALTO/DUACS (Segment Sol multi-missions dALTimetrie, d'Orbitographie et de localisation précise/Data Unification and Altimeter Combination System) and distributed by AVISO+ (http://www.aviso.altimetry.fr/) with support from the Centre National d'Études Spatiales (CNES), in collaboration with Oregon State University with support from the National Aeronautics and Space Administration.

DMK would like to thank Professor J. J. McCarthy for his leadership of JGOFS (Joint Global Ocean Flux Study) that led to the establishment of Station ALOHA in 1988, and for his sage guidance and support of the Hawaii Ocean Time-series program over the past three decades.

APPENDIX

a. Mesoscale eddies at Station ALOHA

We analyzed the characteristics and trajectory of mesoscale eddies to test two hypotheses: (1) that the correlations reported in Table 1 are attributable entirely to mesoscale eddies and (2) that eddies of different polarity originate from different regions of the ocean before arriving at Station ALOHA.

Eddy characteristics and trajectories were obtained from AVISO+ in the form of the global Mesoscale Eddy Trajectory Atlas (version 2.0). The atlas includes all mesoscale eddies detected by a modification of the "growing method" for eddy identification and tracking (Schlax and Chelton 2016). Eddies are reported with daily temporal resolution, and only eddies that lasted for 28 days or more are included. Those eddies are characterized by a set of parameters including the following:

- Coordinates (° N and ° W) of the eddy centroid based on sea surface height (SSH)
- Amplitude (cm), defined as the difference in SSH between the minimum/maximum and the edge of the eddy
- Radius (km), defined as the radius of a circle having the same area as the contour of maximum average geostrophic speed

We calculated the following additional parameters:

- Age (d), defined as the time from the first day of eddy detection
- Amplitude change (cm d^{-1}), defined as the rate of change of eddy amplitude from the previous day
- Horizontal displacement (km d^{-1}), defined as the distance between the position of the eddy centroid from the centroid on the previous day

We defined eddies traversing Station ALOHA as those having a radius greater than the distance between the eddy centroid and the center of the sampling station (22°45′ N, 158° W). This selection was done on a daily basis, so that each eddy traversed Station ALOHA for only a fraction of its lifetime. We excluded those eddies that traversed Station ALOHA but were south of the line connecting points with coordinates 22°18′ N, 159°30′ W and 20°54′ N, 156° W to prevent Station ALOHA to be considered inside eddies whose centroid was southwest of the Hawaiian Islands. We only analyzed the characteristics of those eddies that included Station ALOHA for at least 1 day. Furthermore, we considered only eddies observed during years from 1994 to 2015 to match the time period considered in the correlation analysis between Hawaii Ocean Time-series (HOT) biogeochemical parameters and satellite-derived sea level anomaly (SLA), but excluding year 1993. The exclusion of year 1993 was based on the consideration that eddy lifetime could have been cut short in the first year of the eddy atlas (i.e., 1993).

Station ALOHA was inside a tracked mesoscale eddy 31% of the days between 1994 and 2015. In the same period, 135 eddies traversed Station ALOHA for at least 1 day: 71 cyclones and 64 anticyclones. The amplitude of eddies traversing Station ALOHA was -6.5 ± 3.9 cm (mean $\pm$ standard deviation) and 7.1 ± 3.9 cm for cyclones and anticyclones, respectively (Fig. A1a). Eddy radius was similar between cyclones and anticyclones and averaged 100 ± 32 km (Fig. A1b). The distribution of the age of eddies at the time when they traversed Station ALOHA is skewed right with a median value of 47 days (Fig. A1c). The median eddy horizontal displacement was 5.6 km d^{-1} (Fig. A1d), with about 4% of the

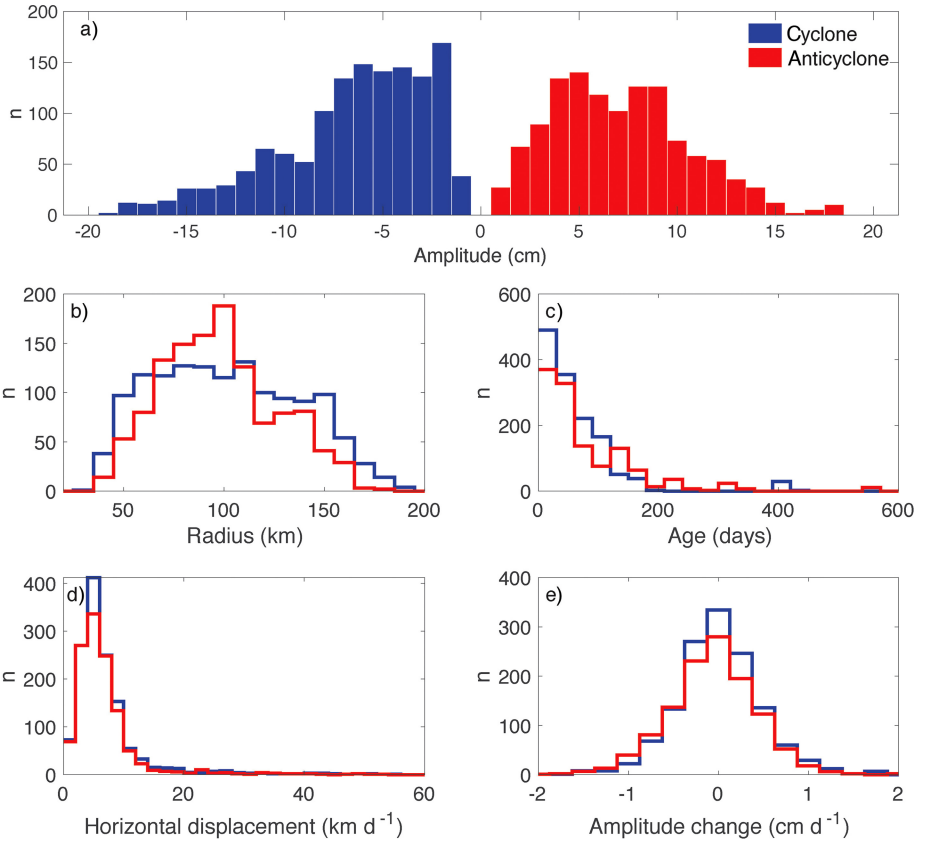

Figure A1. Characteristics of the mesoscale eddies when they traversed the center of Station ALOHA: (a) amplitude, (b) radius, (c) days from first detection, (d) horizontal displacement from the previous day, and (e) change in eddy amplitude from the previous day. Red depicts anticyclones, and blue depicts cyclones.

values above 20 km d^{-1} that could be because of artifacts generated by the eddy-tracking algorithm. Eddy amplitude varied by one day to the next by 0.0 ± 0.5 cm d^{-1} (Fig. A1e).

Days when Station ALOHA was inside one of the tracked eddies accounted for 47% of the variance of SLA_{corr} of the entire time series (Fig. 3). In order to understand if the correlations reported in Table 1 were only detected inside the eddies identified by the tracking procedure, we partitioned the time series into two subsets of observations made of days when Station ALOHA was traversed by a mesoscale eddy and of days when no eddy was detected. We then calculated the correlations reported in Table 1 for the two subsets of measurements (Tables A1 and A2). Results from both subsets of measurements show very similar correlations as those reported for the entire data set in Table 1 (Tables A1 and A2).

Table A1. Correlation coefficients of biogeochemical parameters versus SLA_{corr} for days when Station ALOHA was inside a mesoscale eddy. A missing value indicates that the relationship is not significant according to the Benjamini and Hochberg (1995) procedure. ^{14}C-PP, primary production estimated through assimilation of ^{14}C-labeled bicarbonate; Chl *a*, fluorometric chlorophyll *a*; DIC, dissolved inorganic carbon; DOC, DON, and DOP, respectively dissolved organic carbon, nitrogen, and phosphorus; Euk. Phy., eukaryotic phytoplankton; Het. Pico., heterotrophic picoplankton; $NO_3^- + NO_2^-$, nitrate plus nitrite; O_2, dissolved oxygen; PC and PN, particulate carbon and nitrogen, respectively; PO_4^{3-}, phosphate; *Proch., Prochlorococcus*; SiO_4^{4-}, silicate; SLA, sea level anomaly; *Syn.*, *Synechococcus*.

	Depth levels							
Biogeochemical parameters	5 m	25 m	45 m	75 m	100 m	125 m	150 m	175 m
$NO_3^- + NO_2^-$					−0.4	−0.42	−0.53	−0.65
PO_4^{3-}	0.29	0.36	0.35				−0.34	−0.58
SiO_4^{4-}						−0.37	−0.55	−0.65
DIC				−0.32		−0.65	−0.49	−0.6
O_2			−0.26					
Chl *a*						0.28	0.31	0.31
PC							0.32	
PN				0.3		0.42	0.45	0.46
DOC				0.59				0.59
DON					0.43	0.49		
DOP								
Het. Pico.				0.43	0.34	0.4	0.45	0.43
Proch.								
Syn.								
Euk. Phy.								
^{14}C-PP								

This similarity indicates that the main biogeochemical changes reported in Table 1 are broadly related to changes in SSH.

Eddies traversing Station ALOHA generally originated east of it and were last detected west of it, but the coordinates of origin and last detection were variable (Fig. 5a). For example, one cyclone and one anticyclone originated east of 130° W, while one cyclone was last detected west of 175° W (Fig. 5a). The average coordinates of eddy origin were 22°44′ N, 155°24′ W for cyclones and 22°56′ N, 154°40′ W for anticyclones (Fig. A2). The average coordinates of last detection were 22°51′ N, 159°41′ W for cyclones and 23°11′ N, 159°36′ W for anticyclones (Fig. A2).

Eddies were also tracked back in time from the day of their first detection at Station ALOHA. We found that eddies of opposite polarity propagated at similar speeds and on average came from a direction almost due east of Station ALOHA (Fig. 5b). The average

Table A2. Correlation coefficients of biogeochemical parameters versus SLA_{corr} for days when Station ALOHA was not inside a mesoscale eddy. A missing value indicates that the relationship is not significant according to the Benjamini and Hochberg (1995) procedure. ^{14}C-PP, primary production estimated through assimilation of ^{14}C-labeled bicarbonate; Chl *a*, fluorometric chlorophyll *a*; DIC, dissolved inorganic carbon; DOC, DON, and DOP, respectively dissolved organic carbon, nitrogen, and phosphorus; Euk. Phy., eukaryotic phytoplankton; Het. Pico., heterotrophic picoplankton; $NO_3^- + NO_2^-$, nitrate plus nitrite; O_2, dissolved oxygen; PC and PN, particulate carbon and nitrogen, respectively; PO_4^{3-}, phosphate; *Proch., Prochlorococcus*; SiO_4^{4-}, silicate; SLA, sea level anomaly; *Syn.*, *Synechococcus*.

	Depth levels							
Biogeochemical parameters	5 m	25 m	45 m	75 m	100 m	125 m	150 m	175 m
$NO_3^- + NO_2^-$						−0.29	−0.58	−0.49
PO_4^{3-}	0.16	0.42	0.31	0.26	0.28		−0.44	−0.45
SiO_4^{4-}				−0.28	−0.3	−0.36	−0.52	−0.54
DIC	−0.29	−0.34	−0.4	−0.45	−0.49	−0.55	−0.33	−0.42
O_2		−0.18	−0.28	−0.18				
Chl *a*								
PC								
PN		0.2			0.21	0.25		0.24
DOC				0.31	0.34	0.36	0.32	0.32
DON								
DOP	0.35				0.26		0.33	
Het. Pico.						0.24	0.34	0.23
Proch.					0.22			
Syn.								−0.28
Euk. Phy.								
^{14}C-PP								

distance of eddies from Station ALOHA 60 days before their arrival was 386 ± 83 km. This distance increased to 813 ± 121 km 150 days before their arrival.

Eddies of different polarity originated and propagated from similar regions of the ocean. For this reason, it is unlikely that they transported different surface water to Station ALOHA. These results are consistent with the conclusions of an earlier analysis (Nolan, 2008) that found similar translation speed and direction for both cyclones and anticyclones passing through Station ALOHA.

b. Additional information on the correlations in Table 1

The biogeochemical parameters used to calculate the correlation coefficients reported in Table 1 were measured during different periods and have a different number of data points. We report the different periods of observations and number of samples in Table A3.

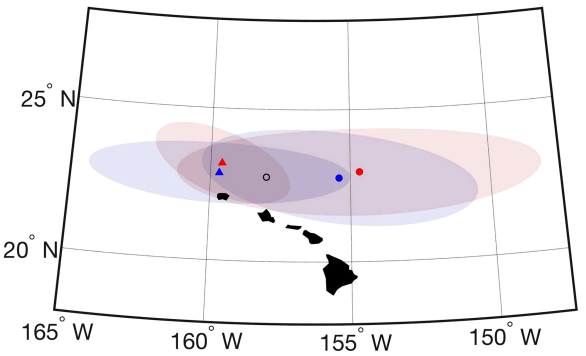

Figure A2. Average coordinates of origin (circles) and last detection (triangles) for cyclones and anticyclones, in blue and red, respectively. Ellipses enclose the region of one standard deviation.

Table A3. Average number of measurements per depth and period of observation for the measurements reported in Table 1. ^{14}C-PP, primary production estimated through assimilation of ^{14}C-labeled bicarbonate; Chl *a*, fluorometric chlorophyll *a*; DIC, dissolved inorganic carbon; DOC, DON, and DOP, respectively dissolved organic carbon, nitrogen, and phosphorus; Euk. Phy., eukaryotic phytoplankton; Het. Pico., heterotrophic picoplankton; $NO_3^- + NO_2^-$, nitrate plus nitrite; O_2, dissolved oxygen; PC and PN, particulate carbon and nitrogen, respectively; PO_4^{3-}, phosphate; *Proch., Prochlorococcus*; SiO_4^{4-}, silicate; *Syn., Synechococcus*.

Biogeochemical parameters	Average number per depth	Period of observation
$NO_3^- + NO_2^-$	213	1993–2015
PO_4^{3-}	213	1993–2015
SiO_4^{4-}	208	1993–2015
DIC	172	1993–2015
O_2	322	1993–2015
Chl *a*	730	1993–2015
PC	209	1993–2014
PN	218	1993–2015
DOC	87	2002–2010
DON	88	1993–2001
DOP	88	1993–2001
Het. Pico.	208	1993–2014
Proch.	209	1993–2014
Syn.	211	1993–2014
Euk. Phy.	210	1993–2014
^{14}C-PP	176	1993–2014

The significance of the correlations in Table 1 was assessed using the Benjamini and Hochberg (1995) procedure for multiple comparisons using a false discovery rate of 0.05. The procedure was applied to the P values reported in Table A4 and obtained from the correlations between SLA_{corr} and the biogeochemical parameters.

c. Autoregression residual analysis

Regression between two observed variables implicitly assumes that the sampled points within each variable are independent. In the HOT data set, the observed variables are time series of biogeochemical quantities (e.g., PO_4^{3-}). These time series likely violate the independence assumption, as the sampled water will have some "memory" or accumulation of, for example, PO_4^{3-} over some timescale.

Let $\mathbf{x} = \{x_1, \ldots, x_N\}$ denote the sampled time series of variable x with N sampled points. For the autoregression step, we define $\mathbf{x}_1 = \{x_1, \ldots, x_{N-1}\}$ and $\mathbf{x}_2 = \{x_2, \ldots, x_N\}$—that is, these are the "earlier" and the "later" time series. We normalize each time series separately by computing the z-score for each measurement i:

$$z_i = \frac{x_i - \mu_x}{\sigma_x}, \tag{A1}$$

where μ_x is the mean and σ_x is the standard deviation of the time series. For the normalized time series $\mathbf{z}$, we use the autoregression (AR) model:

$$z_i = \alpha z_{i-1} + \epsilon_i. \tag{A2}$$

We estimate

$$\alpha = \frac{\sum_{i=2}^{N} z_i z_{i-1}}{\sum_{i=1}^{N-1} z_i^2}, \tag{A3}$$

which we then use to calculate the residuals $\boldsymbol{\epsilon} = \{\epsilon_2, \ldots, \epsilon_N\}$ in equation (A2).

In this AR model, the next output z_i depends only on an independent noise term, and the previous output z_{i-1}, commonly denoted as AR(1). In other words, the system has "memory" between consecutive time points, as measured by α. If $\alpha = 0$, then the variable has no memory, whereas if $\alpha = 1$, then the variable has a long memory (as much as a random walk). It is important to note that if a variable (e.g., PO_4^{3-}), has a long decay time compared with the sampling frequency, a higher-order AR model will be more appropriate.

It is important here to note that the HOT time series does not have evenly spaced samples (Fig. A3). Sampling is approximately monthly, but sometimes shorter (on the order of days) or longer (2 to 3 months or even several years). This means that the assumptions of the AR model may be violated. For example, if the variable (e.g., PO_4^{3-}) has "memory" of 1 month, sample points that are 2 months apart may actually be independent. The effect of uneven sampling times will need to be more carefully considered for future analysis. Here, we used the autoregression residuals of the biogeochemical variable as the dependent

Table A4. *P* values for the correlations reported in Table 1. ^{14}C-PP, primary production estimated through assimilation of ^{14}C-labeled bicarbonate; Chl *a*, fluorometric chlorophyll *a*; DIC, dissolved inorganic carbon; DOC, DON, and DOP, respectively dissolved organic carbon, nitrogen, and phosphorus; Euk. Phy., eukaryotic phytoplankton; Het. Pico., heterotrophic picoplankton; $NO_3^- + NO_2^-$, nitrate plus nitrite; O_2, dissolved oxygen; PC and PN, particulate carbon and nitrogen, respectively; PO_4^{3-}, phosphate; *Proch., Prochlorococcus*; SiO_4^{4-}, silicate; *Syn., Synechococcus*.

Biogeochemical parameters	Depth levels							
	5 m	25 m	45 m	75 m	100 m	125 m	150 m	175 m
$NO_3^- + NO_2^-$	0.56	0.81	0.95	0.52	1.6×10^{-4}	2.1×10^{-6}	8.8×10^{-17}	1.6×10^{-14}
PO_4^{3-}	3.6×10^{-6}	5.4×10^{-8}	5.1×10^{-6}	7.4×10^{-5}	8.7×10^{-4}	0.23	1.1×10^{-8}	2.1×10^{-11}
SiO_4^{4-}	0.46	0.033	0.95	0.0011	0.0025	3.4×10^{-7}	1.1×10^{-14}	2.9×10^{-16}
DIC	0.0014	4.9×10^{-5}	3.0×10^{-7}	2.0×10^{-9}	2.5×10^{-8}	3.0×10^{-6}	4.9×10^{-9}	3.3×10^{-5}
O_2	0.062	0.035	7.5×10^{-6}	0.032	0.39	0.39	0.0062	0.5
Chl *a*	0.88	0.97	0.18	0.14	0.058	6.2×10^{-4}	4.0×10^{-4}	7.2×10^{-4}
PC	0.52	0.12	0.82	0.016	0.023	0.0076	0.022	0.0042
PN	0.29	0.022	0.25	0.004	0.0013	1.6×10^{-6}	8.6×10^{-5}	1.1×10^{-6}
DOC	0.17	0.71	0.0072	4.7×10^{-4}	4.8×10^{-4}	8.2×10^{-5}	0.0013	3.1×10^{-4}
DON	0.11	0.19	0.03	0.023	0.0086	7.0×10^{-4}	0.0018	0.031
DOP	0.049	0.06	0.078	0.17	0.0014	0.018	0.02	0.0088
Het. Pico.	0.047	0.0085	0.0057	4.3×10^{-4}	0.0016	3.2×10^{-5}	2.4×10^{-8}	2.8×10^{-5}
Proch.	0.82	0.91	0.7	0.077	3.2×10^{-4}	0.013	0.062	0.13
Syn.	0.74	0.43	0.34	0.75	0.0081	0.16	0.93	0.069
Euk. Phy.	0.91	0.48	0.95	0.28	0.0033	0.94	0.032	0.063
^{14}C-PP	0.044	0.71	0.42	0.86	0.59	0.072	0.096	0.57

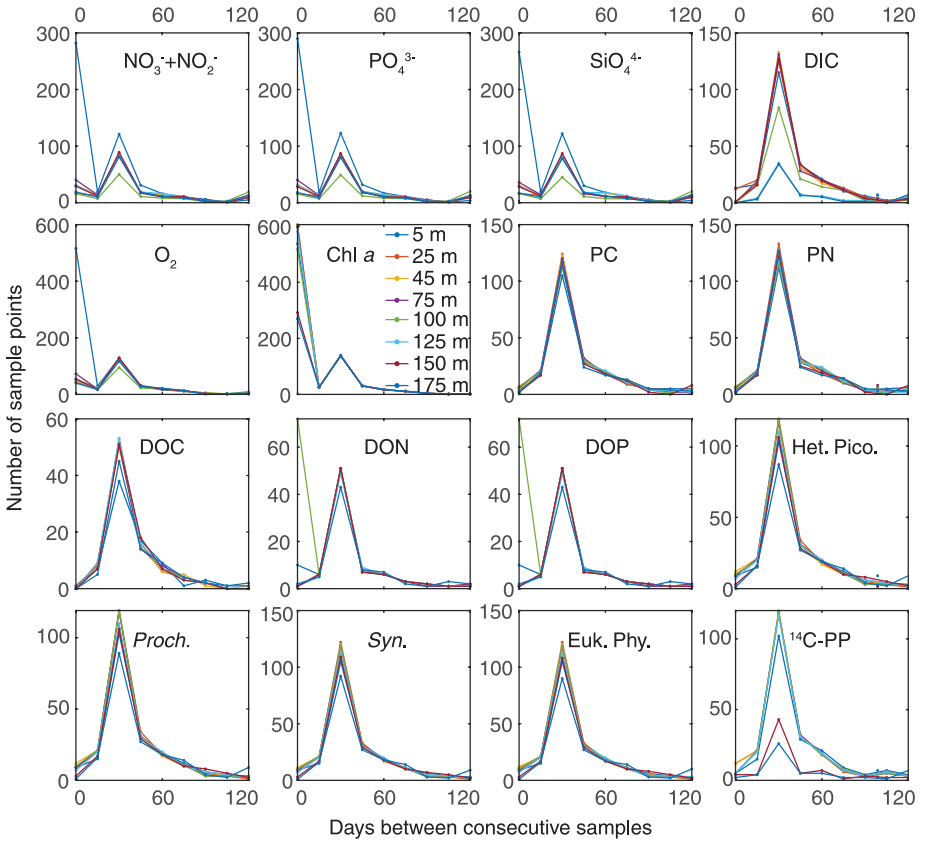

Figure A3. Histogram of days between consecutive sample points for each variable. Each line color is a different sampling depth (e.g., green = 100 m). Typically, the majority of samples are 30 days apart. However, for a few variables at certain depths (e.g., DOP at 100 m), the sampling frequency is less consistent, with most of the samples less than 15 days apart. The last bin (120 days) also includes all sample times greater than 120 days. A few variables have greater than 1 year between consecutive samples. ^{14}C-PP, primary production estimated through assimilation of ^{14}C-labeled bicarbonate; Chl *a*, fluorometric chlorophyll *a*; DIC, dissolved inorganic carbon; DOC, DON, and DOP, respectively dissolved organic carbon, nitrogen, and phosphorus; Euk. Phy., eukaryotic phytoplankton; Het. Pico., heterotrophic picoplankton; $NO_3^- + NO_2^-$, nitrate plus nitrite; O_2, dissolved oxygen; PC and PN, particulate carbon and nitrogen, respectively; PO_4^{3-}, phosphate; *Proch., Prochlorococcus*; SiO_4^{4-}, silicate; *Syn., Synechococcus*.

variable and the residuals of SLA_{corr} as the independent variable. Results from this analysis (Table A5) are largely in agreement with results in the main text. Out of 65 significant correlations in the original analysis (Table 1), 61 were significant and had the same sign in the autoregression residual analysis (Table A5). Furthermore, 11 correlations were only

Table A5. Correlation coefficients of biogeochemical autoregression residuals versus SLA_{corr} autoregression residuals. A missing value indicates that the relationship is not significant according to the Benjamini and Hochberg (1995) procedure. ^{14}C-PP, primary production estimated through assimilation of ^{14}C-labeled bicarbonate; Chl *a*, fluorometric chlorophyll *a*; DIC, dissolved inorganic carbon; DOC, DON, and DOP, respectively dissolved organic carbon, nitrogen, and phosphorus; Euk. Phy., eukaryotic phytoplankton; Het. Pico., heterotrophic picoplankton; $NO_3^- + NO_2^-$, nitrate plus nitrite; O_2, dissolved oxygen; PC and PN, particulate carbon and nitrogen, respectively; PO_4^{3-}, phosphate; *Proch., Prochlorococcus*; SiO_4^{4-}, silicate; SLA, sea level anomaly; *Syn., Synechococcus*.

	Depth levels							
Biogeochemical parameters	5 m	25 m	45 m	75 m	100 m	125 m	150 m	175 m
$NO_3^- + NO_2^-$					−0.32	−0.37	−0.59	−0.55
PO_4^{3-}	0.16	0.39	0.39	0.29	0.23		−0.43	−0.49
SiO_4^{4-}		0.19		−0.27	−0.31	−0.37	−0.58	−0.6
DIC	−0.2	−0.25	−0.42	−0.51	−0.52	−0.57	−0.47	−0.51
O_2		−0.14	−0.27	−0.13			0.22	
Chl *a*						0.09	0.15	0.18
PC						0.18	0.16	0.25
PN					0.2	0.32	0.27	0.35
DOC			0.28	0.35	0.36	0.39	0.3	0.39
DON			0.25	0.26	0.21	0.39	0.38	0.27
DOP			0.29		0.27	0.28	0.31	0.32
Het. Pico.		0.15	0.17	0.16	0.18	0.24	0.36	0.38
Proch.				0.16	0.24	0.18		
Syn.					0.18			
Euk. Phy.					−0.19			0.18
^{14}C-PP	−0.18					0.16		

significant in the autoregression residual analysis. The consistency between the original analysis and the autoregression residual analysis reinforces the observed trends including the correlation between PO_4^{3-} and SLA_{corr} switching from positive to negative with depth.

d. Diapycnal and isopycnal mixing

Changes in the phytoplankton community composition with SSH at the depth of the DCM (Table 1) can be linked to changes in nutrient supply because of turbulent diffusion. We here estimate the magnitude of the changes of turbulent fluxes at 100 m between conditions of low and high SSH, and we compare the magnitude of fluxes in the diapycnal and isopycnal direction. Our calculations are similar to those done by Siegel, McGillicuddy, and Fields (1999) for the Atlantic Ocean with one major difference: Siegel, McGillicuddy, and Fields (1999) aimed to estimate the diffusive flux of nutrients into the euphotic zone on an areal basis; we aim to calculate nutrient diffusion in a specific layer of water, centered at 100 m depth,

on a volumetric basis. For this reason, while Siegel, McGillicuddy, and Fields (1999) estimated areal fluxes using the first spatial derivatives of nutrient concentrations, we estimated volumetric fluxes using the second spatial derivatives according to Fick's second law.

The rate of turbulent diffusion of a nutrient C in or out of a parcel of water is the sum of two terms:

$$K_z \frac{\partial^2 C}{\partial z^2} + K_i \left(\frac{\partial^2 C}{\partial x^2} + \frac{\partial^2 C}{\partial y^2} \right), \tag{A4}$$

where the left term is the diapycnal component, and the right term is the isopycnal component. Diapycnal diffusion is regulated by the vertical eddy diffusivity, K_z, and the second vertical derivative of C. Isopycnal diffusion is regulated by the isopycnal eddy diffusivity, K_i, and by the second horizontal derivatives of the isopycnal concentration of C in the zonal, x, and meridional, y, directions. As a consequence, we can test if the rate of NO_3^- + NO_2^- diffusion changes with SLA_{corr} by looking at changes in the second spatial derivatives of the concentration of these inorganic nutrients.

For vertical concentration gradients, we can compute the second derivative using finite differences on the median profiles of Figure 4(a). This calculation shows that for $SLA_{corr} < -5$ cm, the second vertical derivative of $NO_3^- + NO_2^-$ was more than threefold greater than for $SLA_{corr} > 5$ cm (0.67 vs. 0.18 nmol kg^{-1} m^{-2}, but we are likely underestimating both values because of the coarse vertical resolution of sampling). Although vertical concentration gradients are routinely measured within HOT, there are no measurements of isopycnal gradients. In order to obtain an estimate for these gradients, we decompose the concentration along an isopycnal into two terms:

$$C(x, y) = f[\mathrm{SLA}(x, y)] + \varepsilon(x, y), \tag{A5}$$

where $f[\mathrm{SLA}(x, y)]$ is the mesoscale variability of C associated with changes in SLA, and $\varepsilon(x, y)$ includes all other sources of variability as the submesoscale or the large scale. Considering our focus on mesoscale changes in diffusive fluxes associated with changes in community composition, we neglect the second term of equation (A5). We can now decompose the second horizontal derivatives of C as follows:

$$\frac{\partial^2 C}{\partial x^2} + \frac{\partial^2 C}{\partial y^2} = \left(\frac{\partial^2 \mathrm{SLA}}{\partial x^2} + \frac{\partial^2 \mathrm{SLA}}{\partial y^2} \right) \frac{\partial C}{\partial \mathrm{SLA}} + \left(\frac{\partial \mathrm{SLA}}{\partial x} \right)^2 \frac{\partial^2 C}{\partial \mathrm{SLA}^2} + \left(\frac{\partial \mathrm{SLA}}{\partial y} \right)^2 \frac{\partial^2 C}{\partial \mathrm{SLA}^2}. \tag{A6}$$

We then express the isopycnal variation of $NO_3^- + NO_2^-$ with SLA as a linear function and we calculate its slope, $\partial C/\partial \mathrm{SLA}$, through regression (Fig. A4b). Under the linear assumption, the last two terms on the right of equation (A6) become zero, and the isopycnal diffusive flux becomes

$$K_i \left(\frac{\partial^2 \mathrm{SLA}}{\partial x^2} + \frac{\partial^2 \mathrm{SLA}}{\partial y^2} \right) \frac{\partial C}{\partial \mathrm{SLA}}. \tag{A7}$$

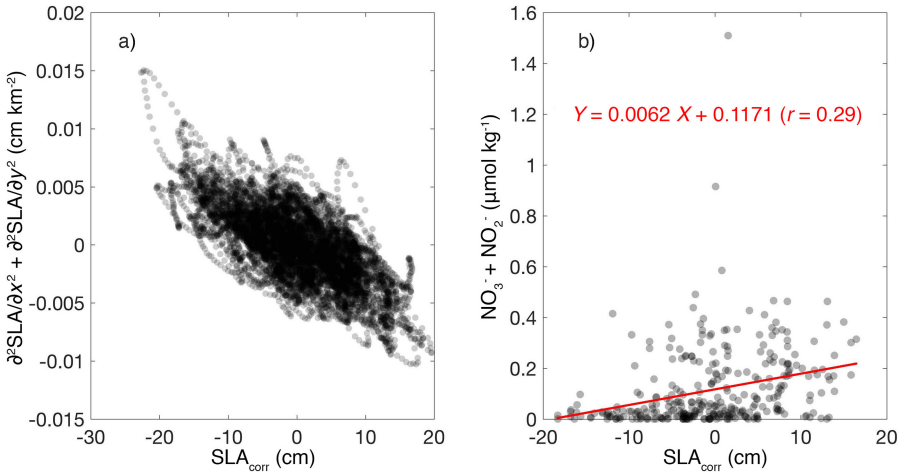

Figure A4. Scatter plots of two parameters used to calculate isopycnal and diapycnal nutrient fluxes. (a) Daily estimates of the second horizontal derivative of sea level anomaly (SLA) at Station ALOHA plotted against SLA_{corr}. (b) Concentration of $NO_3^- + NO_2^-$ on the 24.22 kg m^{-3} isopycnal against SLA_{corr}. The red line in panel (b) is the result of the linear regression. Model I regression was chosen rather than model II to prevent the fitted line from assuming negative concentration values.

The zonal and meridional second derivatives of SLA can then be calculated from SLA maps using the finite difference method on one point and its two neighbor points on each axis. Results from this calculation show that the total second horizontal derivative of SLA at Station ALOHA is inversely proportional to SLA_{corr} (Fig. A4a) and on average is positive for negative values of SLA_{corr}, and negative for positive values of SLA_{corr}. This means that the sea surface tends to change from concave to convex when SLA_{corr} changes sign with a consequent change in the sign of the isopycnal diffusive flux. The term $\partial C/\partial SLA$ was estimated for variation of $NO_3^- + NO_2^-$ on the isopycnal with a potential density anomaly of 24.22 kg m^{-3} that on average lies at 100 m depth during HOT. The linear regression slope was found to be 0.0062 µmol kg^{-1} cm^{-1} (Fig. A4b).

At this point, we have estimates for both isopycnal and diapycnal second derivatives of $NO_3^- + NO_2^-$, and we can compare the magnitude of the two diffusive rates under the assumption of a value for K_z and K_i. Because of the uncertainty in the values of both eddy diffusivities, we can only obtain approximations of the diffusive fluxes, and we did so by assuming that $K_i = 1$ m^2 s^{-1} (Shcherbina et al. 2015) and that $K_z = 10^{-5}$ m^2 s^{-1} (Ledwell, Watson, and Law 1993). The resulting isopycnal fluxes are two orders of magnitude weaker than diapycnal fluxes (Table A6), so we conclude that the latter are most likely responsible for the increased abundance of eukaryotic phytoplankton at 100 m depth at low SLA_{corr}.

Table A6. Estimates for the terms in equations (A4) and (A7) at high and low SLA_{corr} for the concentration of $NO_3^- + NO_2^-$. SLA, sea level anomaly.

Terms	Units	$SLA_{corr} < -5$ cm	$SLA_{corr} > 5$ cm
$\partial^2 SLA/\partial x^2 + \partial^2 SLA/\partial y^2$	cm km^{-2}	0.0027	−0.0028
$\partial C/\partial SLA$	μmol kg^{-1} cm^{-1}	0.0062	0.0062
$\partial^2 C/\partial x^2 + \partial^2 C/\partial y^2$	μmol kg^{-1} km^{-2}	1.7×10^{-5}	-1.7×10^{-5}
$\partial^2 C/\partial z^2$	μmol kg^{-1} m^{-2}	6.7×10^{-4}	1.8×10^{-4}
Isopycnal diffusion ($K_i = 1$ m^2 s^{-1})	μmol kg^{-1} d^{-1}	1.5×10^{-6}	-1.5×10^{-6}
Diapycnal diffusion ($K_z = 10^{-5}$ m^2 s^{-1})	μmol kg^{-1} d^{-1}	5.8×10^{-4}	1.5×10^{-4}

e. Nitrogen fluxes caused by isopycnal uplift and diapycnal mixing

In the previous section, we showed how increased diapycnal fluxes of nitrogen sustain a more abundant eukaryotic community at the DCM. However, our calculations do not indicate that diapycnal diffusion was the largest nitrogen flux in the euphotic zone linked to changes in SSH. Instead, upwelling appeared to be an important flux of inorganic nutrients, when SSH decreased and isopycnals were uplifted. We therefore estimate and compare nitrogen fluxes in the euphotic zone resulting from isopycnal uplift and diapycnal mixing, in order to assess their relative importance. For this purpose, a flux to the euphotic zone was defined as an input of $NO_3^- + NO_2^-$ in the 0–100 m depth layer, where $NO_3^- + NO_2^-$ concentration was persistently low (Table 2).

We estimated the flux of nitrogen caused by isopycnal uplift by first calculating the ideal vertical profile of $NO_3^- + NO_2^-$ that we would observe at low SSH ($SLA_{corr} < -5$ cm) if we translated vertically the median concentrations observed in neutral SSH conditions (SLA_{corr} between −5 and 5 cm). For this calculation, we shifted the vertical profile toward shallower depths by a length dictated by the slopes of Figure 2 and the change in SSH between low and neutral SSH conditions (9.5 cm). We then compared this translated profile to the median profile observed in conditions of low SSH ($SLA_{corr} < -5$ cm). The difference in the 0–100 m integral concentration of $NO_3^- + NO_2^-$ between the translated neutral profile and the profile at low SSH represents the nitrogen that had been uplifted in the euphotic zone and was removed through biological consumption. In this way, we calculated that isopycnal uplift caused a flux of 4.4 mmol m^{-2} $NO_3^- + NO_2^-$ above 100 m, in conditions of low SSH.

Diapycnal nitrogen fluxes in the euphotic zone resulting from changes in SSH can be estimated based on the difference in vertical gradients of $NO_3^- + NO_2^-$ at the base of the euphotic zone (here defined as the 100–150 m depth layer). This vertical gradient changed from 29 μmol m^{-4} in conditions of low SSH ($SLA_{corr} < -5$ cm), $\frac{\partial N}{\partial z}_{low}$, to 18 μmol m^{-4} in neutral conditions (SLA_{corr} between −5 and 5 cm), $\frac{\partial N}{\partial z}_{neutr}$. The difference between these vertical gradients multiplied by the vertical eddy diffusivity, K_z, and the duration of

gradient intensification, τ, represent the diapycnal nitrogen flux at the base of the euphotic zone associated with changes in SSH, F_{dia}:

$$F_{\text{dia}} = \left(\frac{\partial N}{\partial z_{\text{low}}} - \frac{\partial N}{\partial z_{\text{neutr}}} \right) K_z \tau. \tag{A8}$$

We then assume that $K_z = 10^{-5}$ m^2 s^{-1} (Ledwell, Watson, and Law 1993) and that vertical gradients are intensified during a period equivalent to the length of the mature phase of a cyclonic eddy. From the data set in Appendix a, we also know that the average lifetime of cyclones in the region of interest was 93 days. We then assume that the mature phase of an eddy lasts for 70% of its life cycle (Samelson, Schlax, and Chelton 2014) resulting in a $\tau = 65$ days. Under these assumptions, the increase in the diapycnal flux at the base of the euphotic zone, F_{dia}, was 0.6 mmol m^{-2} NO_3^- + NO_2^-.

Our calculations show that the upwelling of NO_3^- + NO_2^- in the euphotic zone caused by isopycnal uplift (4.4 mmol m^{-2}) was larger than the nitrogen flux caused by increased diapycnal diffusion (0.6 mmol m^{-2}) in conditions of low SSH.

REFERENCES

Ascani, F., K. J. Richards, E. Firing, S. Grant, K. S. Johnson, Y. Jia, R. Lukas, and D. M. Karl. 2013. Physical and biological controls of nitrate concentrations in the upper subtropical North Pacific Ocean. Deep-Sea Res., Part II, *93*, 119–134. doi: 10.1016/j.dsr2.2013.01.034

Benitez-Nelson, C. R., R. R. Bidigare, T. D. Dickey, M. R. Landry, C. L. Leonard, S. L. Brown, F. Nencioli, et al. 2007. Mesoscale eddies drive increased silica export in the subtropical Pacific Ocean. Science, *316*, 1017–1021. doi: 10.1126/science.1136221

Benjamini, Y., and Y. Hochberg. 1995. Controlling the false discovery rate: A practical and powerful approach to multiple testing. J. R. Stat. Soc., Ser. B, *57*, 289–300. doi: 10.2307/2346101

Chelton, D. B., and M. G. Schlax. 1996. Global observations of oceanic Rossby waves. Science, *272*, 234–238. doi: 10.1126/science.272.5259.234

Chelton, D. B., M. G. Schlax, and R. M. Samelson. 2011. Global observations of nonlinear mesoscale eddies. Prog. Oceanogr., *91*, 167–216. doi: 10.1016/j.pocean.2011.01.002

Chiswell, S. M. 1996. Intra-annual oscillations at Station ALOHA, north of Oahu, Hawaii. Deep-Sea Res., Part II, *43*, 305–319. doi: 10.1016/0967-0645(95)00089-5

Church, J. A., P. U. Clark, A. Cazenave, J. M. Gregory, S. Jevrejeva, A. Levermann, M. A. Merrifield, et al. 2013. Sea level change, *in* Climate Change 2013: The Physical Science Basis. Contribution of Working Group I to the Fifth Assessment Report of the Intergovernmental Panel on Climate Change, T. F. Stocker, D. Qin, G.-K. Plattner, M. Tignor, S. K. Allen, J. Boschung, A. Nauels, Y. Xia, V. Bex, and P. M. Midgley, eds. Cambridge: Cambridge University Press, 1137–1216.

Church, M. J., C. Mahaffey, R. M. Letelier, R. Lukas, J. P. Zehr, and D. M. Karl. 2009. Physical forcing of nitrogen fixation and diazotroph community structure in the North Pacific subtropical gyre. Global Biogeochem. Cycles, *23*, GB2020. doi: 10.1029/2008GB003418

de Boyer Montégut, C., G. Madec, A. S. Fischer, A. Lazar, and D. Iudicone. 2004. Mixed layer depth over the global ocean: An examination of profile data and a profile-based climatology. J. Geophys. Res.: Oceans, *109*, C12003. doi: 10.1029/2004JC002378

Doney, S. C., D. M. Glover, S. J. McCue, and M. Fuentes. 2003. Mesoscale variability of Sea-viewing Wide Field-of-view Sensor (SeaWiFS) satellite ocean color: Global patterns and spatial scales. J. Geophys. Res., *108*(C2), 3024. doi: 10.1029/2001JC000843

Eden, B. R., D. K. Steinberg, S. A. Goldthwait, and D. J. McGillicuddy. 2009. Zooplankton community structure in a cyclonic and mode-water eddy in the Sargasso Sea. Deep-Sea Res., Part I, *56*, 1757–1776. doi: 10.1016/j.dsr.2009.05.005

Falkowski, P. G., D. Ziemann, Z. Kolber, and P. K. Bienfang. 1991. Role of eddy pumping in enhancing primary production in the ocean. Nature, *352*, 55–58. doi: 10.1038/352055a0

Fang, M., and J. Zhang. 2015. Basin-scale features of global sea level trends revealed by altimeter data from 1993 to 2013. J. Oceanogr., *71*, 297–310. doi: 10.1007/s10872-015-0289-1

Fawcett, S. E., M. W. Lomas, J. R. Casey, B. B. Ward, and D. M. Sigman. 2011. Assimilation of upwelled nitrate by small eukaryotes in the Sargasso Sea. Nat. Geosci., *4*, 717–722. doi: 10.1038/ngeo1265

Hannides, C. C. S., J. C. Drazen, and B. N. Popp. 2015. Mesopelagic zooplankton metabolic demand in the North Pacific Subtropical Gyre. Limnol. Oceanogr., *60*, 419–428. doi: 10.1002/lno.10032

Karl, D. M., and R. Lukas. 1996. The Hawaii Ocean Time-series (HOT) program: Background, rationale and field implementation. Deep-Sea Res., Part II, *43*, 129–156. doi: 10.1016/0967-0645(96)00005-7

Landry, M. R., M. Decima, M. P. Simmons, C. C. S. Hannides, and E. Daniels. 2008. Mesozooplankton biomass and grazing responses to Cyclone Opal, a subtropical mesoscale eddy. Deep-Sea Res., Part II, *55*, 1378–1388. doi: 10.1016/j.dsr2.2008.01.005

Ledwell, J. R., A. J. Watson, and C. S. Law. 1993. Evidence for slow mixing across the pycnocline from an open-ocean tracer-release experiment. Nature, *364*, 701–703. doi: 10.1038/364701a0

McGillicuddy, D. J., L. A. Anderson, N. R. Bates, T. Bibby, K. O. Buesseler, C. A. Carlson, C. S. Davis, et al. 2007. Eddy/wind interactions stimulate extraordinary mid-ocean plankton blooms. Science, *316*, 1021–1026. doi: 10.1126/science.1136256

McGillicuddy, D. J., A. R. Robinson, D. A. Siegel, H. W. Jannasch, R. Johnson, T. D. Dickey, J. McNeil, A. F. Michaels, and A. H. Knap. 1998. Influence of mesoscale eddies on new production in the Sargasso Sea. Nature, *394*, 263–266. doi: 10.1038/28367

McWilliams, J. C. 1974. MODE mean currents and eddy surface intensification. MODE Hotline News, *57*, 1–6.

Mitchum, G. T. 1996. On using satellite altimetric heights to provide a spatial context for the Hawaii Ocean Time-series measurements. Deep-Sea Res., Part II, *43*, 257–280. doi: 10.1016/0967-0645(95)00091-7

Morrow, R., and P.-Y. Le Traon. 2012. Recent advances in observing mesoscale ocean dynamics with satellite altimetry. Adv. Space Res., *50*, 1062–1076. doi: 10.1016/j.asr.2011.09.033

Munk, W. 2002. The evolution of physical oceanography in the last hundred years. Oceanography, *15*, 135–141. doi: 10.5670/oceanog.2002.45

Nolan, K. M. 2008. Characteristics and Water Properties of Mesoscale Eddies in the Region of Station ALOHA. MS thesis. Honolulu: University of Hawaii at Manoa.

Pedlosky, J. 1979. Geophysical Fluid Dynamics. New York: Springer-Verlag.

Robinson, A. R., D. J. McGillicuddy, J. Calman, H. W. Ducklow, M. J. R. Fasham, F. E. Hoge, W. G. Leslie, et al. 1993. Mesoscale and upper ocean variabilities during the 1989 JGOFS bloom study. Deep-Sea Res., Part II, *40*, 9–35. doi: 10.1016/0967-0645(93)90004-7

Samelson, R. M., M. G. Schlax, and D. B. Chelton. 2014. Randomness, symmetry, and scaling of mesoscale eddy life cycles. J. Phys. Oceanogr., *44*, 1012–1029. doi: 10.1175/JPO-D-13-0161.1

Schlax, M. G., and D. B. Chelton. 2016. The "Growing Method" of Eddy Identification and Tracking in Two and Three Dimensions. Corvallis: College of Earth, Ocean and Atmospheric Sciences, Oregon State University.

Shcherbina, A. Y., M. A. Sundermeyer, E. Kunze, E. D'Asaro, G. Badin, D. Birch, A.-M. E. G. Brunner-Suzuki, et al. 2015. The LatMix summer campaign: Submesoscale stirring

in the upper ocean. Bull. Am. Meteorol. Soc., *96*, 1257–1279. doi: 10.1175/BAMS-D-14-00015.1

Siegel, D. A., D. J. McGillicuddy, and E. A. Fields. 1999. Mesoscale eddies, satellite altimetry, and new production in the Sargasso Sea. J. Geophys. Res.: Oceans, *104*, 13359–13379. doi: 10.1029/1999JC900051

Sweeney, E. N., D. J. McGillicuddy, and K. O. Buesseler. 2003. Biogeochemical impacts due to mesoscale eddy activity in the Sargasso Sea as measured at the Bermuda Atlantic Time-series Study (BATS). Deep-Sea Res., Part II, *50*, 3017–3039. doi: 10.1016/j.dsr2.2003.07.008

Uz, B. M., J. A. Yoder, and V. Osychny. 2001. Pumping of nutrients to ocean surface waters by the action of propagating planetary waves. Nature, *409*, 597–600. doi: 10.1038/35054527

Vinogradov, S. V., and R. M. Ponte. 2010. Annual cycle in coastal sea level from tide gauges and altimetry. J. Geophys. Res.: Oceans, *115*, C04021. doi: 10.1029/2009JC005767

Wunsch, C. 1997. The vertical partition of oceanic horizontal kinetic energy. J. Phys. Oceanogr., *27*, 1770–1794. doi: 10.1175/1520-0485(1997)027<1770:TVPOOH>2.0.CO;2

Wyrtki, K. 1990. Sea level rise: The facts and the future. Pacific Sci., *44*, 1–16.

Zhang, Z., W. Wang, and B. Qiu. 2014. Oceanic mass transport by mesoscale eddies. Science, *345*, 322–324. doi: 10.1126/science.1252418

Received: *15 April 2019*; revised: *1 July 2019*.